Applications of a nonlinear evolution equation II: the EMC effect

Xurong Chen[1], **Jianhong Ruan**[2], **Rong Wang**[1,3]
Pengming Zhang[1] and **Wei Zhu**[2*]

[1]Institute of Modern Physics, Chinese Academy of Sciences, Lanzhou 730000, P.R. China
[2]Department of Physics, East China Normal University, Shanghai 200062, P.R. China
[3] University of Chinese Academy of Sciences, Beijing, 100049, P.R. China

Abstract

The EMC effect is studied by using the DGLAP equation with the ZRS corrections and minimum number of free parameters, where the nuclear shadowing effect is a dynamical evolution result of the equation, the nucleon swelling and Fermi motion in the nuclear environment deform the input parton distributions. Parton distributions of both proton and nucleus are predicted in a unified framework. We show that the parton recombination as a higher twist correction plays an essential role in the evolution of parton distributions either of proton or nucleus. We find that the nuclear anti-shadowing contributes a part of enhancement of the ratio of the structure functions around $x \sim 0.1$, while the other part origins from the deformation of the nuclear valence quark distributions. In particularly, the nuclear gluon distributions are dynamically predicted, which are important information for the recherche of the high energy nuclear physics.

PACS number(s):13.60.Hb; 12.38.Bx

keywords: EMC effect, Nuclear shadowing and anti-shadowing, QCD evolution equation; Nonlinear corrections

*Corresponding author, E-mail: weizhu@mail.ecnu.edu.cn

1 Introduction

The question that how the properties of hadrons bounded in nuclear medium differ from that of free hadrons is an important and active research topic of experiment and theory. Example of such medium modifications is the European Muon Collaboration (EMC) effect in the deep-inelastic scattering (DIS), which has been discussed extensively since early 1980s starting from the observation of a change in the structure function of a heavy nucleus relative to that of the deuteron [1]. The nuclear effects in DIS were further measured in the form of the ratio $R(A/B) = F_2^A/F_2^B$ of two nuclei. From the studies of data on the ratio R(A/B) one can divide a few regions of characteristic nuclear effects [2]: depletion of nuclear structure functions at small Bjorken variable $x \lesssim 0.05$ (shadowing region); a small enhancement of nuclear structure functions for $0.05 \lesssim x \lesssim 0.3$ (anti-shadowing); depletion with a minimum around $x = 0.6 \sim 0.7$ (known as EMC effect) followed by a rise at large x (Fermi motion).

A quantitative understanding of the EMC effect can help us to understand how the properties of hadrons are modified in a nuclear medium and even can provide valuable insights into the origin of nuclear force. In particular, the EMC effect has been taken as fundamental basis in establishing the nuclear parton distributions, which often serve as the source of information about quark-gluon plasma (QGP) and color glass condensation (CGC) in heavy ion collisions at the BNL Relativistic Heavy Ion Collider (RHIC) and the CERN Large Hadron Collider (LHC). For these sakes, a proper theory of the EMC effect should explain not only the ratios of the structure functions but also the absolute values of the nuclear structure functions themselves.

The complexity of the EMC effect is due to the fact that the parton distributions of a bound nucleon are affected through both perturbative and nonperturbative ways. The parton recombination is generally thought as a source of the nuclear shadowing, which can be described in a perturbative framework. Close, Qiu and Roberts described the nuclear shadowing using a perturbative QCD calculation of the gluon recombination function at a fixed Q^2 scale in [3]. This work is irrelevant to any dynamical equation and is less in the prediction power. Mueller and Qiu used the DGLAP equation with the GLR-MQ corrections discussed qualitatively the nuclear shadowing in [4, 5]. In our previous work [6] we obtained the parton distribution functions of the proton, which are evaluated dynamically using the DGLAP equation with the ZRS corrections [7–9] from a low scale, where the nucleon consists valence quarks. The simple input distributions of the proton can describe the nonperturbative nuclear corrections. The above scheme allows us to dynamically and quantitatively research the EMC effect. For this sake, in this paper we first generalize the ZRS corrections to the deep inelastic scattering off a nuclear target in Sec. 2. We find that the nuclear shadowing effect is a dynamical result of the parton recombination due to multi-nucleon correlations in the nuclear target. Then we add the

contributions of a traditional Fermi motion and the nucleon swelling on the nuclear input parton distributions in Secs. 3 and 4, respectively. A series of the EMC effect ratios are presented in Sec. 5, which are consistent with the present experimental data. We also calculate the anti-shadowing effect and point out that the so-called anti-shadowing effect is mainly due to the deformation of the valence quarks in a swelling nucleon rather than a compensation to the shadowing correction. In particularly, the nuclear gluon distributions are dynamically predicted in Figs. 6 and 7, which are important information in studying high energy nuclear physics. The discussions and summary are given in the Sec. 6.

2 Dynamical nuclear shadowing

The corrections of parton recombination to the QCD evolution of the parton distributions in proton have been studied with the ZSR equation. In nuclear target, the longitudinal localization size of a parton with small x could exceed a nucleon size. In this case, the partons in different nucleons could interact and they contribute a factor A_{eff} in the following modified DGLAP equation with the ZRS corrections [7–9]. We define that $f^A_{v_j}(x,Q^2)$ (j=u,d) are valence quark distributions, $f^A_{q_i}(x,Q^2)$ (i=u,d,s) are sea quark distributions, $f^A_{\overline{q}_i}(x,Q^2)$ (i=u,d,s) are anti-sea quark distributions and $f^A_g(x,Q^2)$ is gluon distribution, $\Sigma^A(x,Q^2) \equiv \sum_j f^A_{v_j}(x,Q^2) + \sum_i f^A_{q_i}(x,Q^2) + \sum_i f^A_{\overline{q}_i}(x,Q^2)$. Thus, the DGLAP equation with the ZRS corrections in nuclear target reads

$$
\begin{aligned}
&Q^2\frac{dxf^A_{v_j}(x,Q^2)}{dQ^2} \\
&= \frac{\alpha_s(Q^2)}{2\pi}\int_x^1 \frac{dy}{y}P_{qq}(z)xf^A_{v_j}(y,Q^2) \\
&-\frac{\alpha_s(Q^2)}{2\pi}xf^A_{v_j}(x,Q^2)\int_0^1 dzP_{qq}(z) \\
&-A_{eff}\frac{\alpha_s^2(Q^2)}{4\pi R^2Q^2}\int_x^{1/2}\frac{dy}{y}xP_{qg\to q}(x,y)yf^A_g(y,Q^2)yf^A_{v_j}(y,Q^2) \\
&+A_{eff}\frac{\alpha_s^2(Q^2)}{4\pi R^2Q^2}\int_{x/2}^{x}\frac{dy}{y}xP_{qg\to q}(x,y)yf^A_g(y,Q^2)yf^A_{v_j}(y,Q^2) \\
&-A_{eff}\frac{\alpha_s^2(Q^2)}{4\pi R^2Q^2}\int_x^{1/2}\frac{dy}{y}xP_{qq\to q}(x,y)y[\Sigma^A(y,Q^2)-f^A_{v_j}(y,Q^2)]yf^A_{v_j}(y,Q^2) \\
&+A_{eff}\frac{\alpha_s^2(Q^2)}{4\pi R^2Q^2}\int_{x/2}^{x}\frac{dy}{y}xP_{qq\to q}(x,y)y[\Sigma^A(y,Q^2)-f^A_{v_j}(y,Q^2)]yf^A_{v_j}(y,Q^2), (if\ x\le 1/2),
\end{aligned}
$$

$$
\begin{aligned}
&Q^2\frac{dxf^A_{v_j}(x,Q^2)}{dQ^2} \\
&= \frac{\alpha_s(Q^2)}{2\pi}\int_x^1 \frac{dy}{y}P_{qq}(z)xf^A_{v_j}(y,Q^2) \\
&-\frac{\alpha_s(Q^2)}{2\pi}xf^A_{v_j}(x,Q^2)\int_0^1 dzP_{qq}(z) \\
&+A_{eff}\frac{\alpha_s^2(Q^2)}{4\pi R^2Q^2}\int_{x/2}^{1/2}\frac{dy}{y}xP_{qg\to q}(x,y)yf^A_g(y,Q^2)yf^A_{v_j}(y,Q^2) \\
&+A_{eff}\frac{\alpha_s^2(Q^2)}{4\pi R^2Q^2}\int_{x/2}^{1/2}\frac{dy}{y}xP_{qq\to q}(x,y)y[\Sigma^A(y,Q^2)-f^A_{v_j}(y,Q^2)]yf^A_{v_j}(y,Q^2), (if\ 1/2\le x\le 1),
\end{aligned}
\tag{1-a}
$$

for valence quarks, where $z = x/y$, the factor $1/(4\pi R^2)$ is from normalizing two-parton distribution, R is the correlation length of two initial partons,

$$
\begin{aligned}
&Q^2\frac{dxf^A_{\overline{q}_i}(x,Q^2)}{dQ^2}\\
&=\frac{\alpha_s(Q^2)}{2\pi}\int_x^1\frac{dy}{y}P_{qq}(z)xf^A_{\overline{q}_i}(y,Q^2)\\
&-\frac{\alpha_s(Q^2)}{2\pi}xf^A_{\overline{q}_i}(x,Q^2)\int_0^1 dzP_{qq}(z)\\
&+\frac{\alpha_s(Q^2)}{2\pi}\int_x^1\frac{dy}{y}P_{qg}(z)xf^A_g(y,Q^2)\\
&-A_{eff}\frac{\alpha_s^2(Q^2)}{4\pi R^2Q^2}\int_x^{1/2}\frac{dy}{y}xP_{gg\to\overline{q}}(x,y)[yf^A_g(y,Q^2)]^2\\
&+A_{eff}\frac{\alpha_s^2(Q^2)}{4\pi R^2Q^2}\int_{x/2}^{x}\frac{dy}{y}xP_{gg\to\overline{q}}(x,y)[yf^A_g(y,Q^2)]^2\\
&-A_{eff}\frac{\alpha_s^2(Q^2)}{4\pi R^2Q^2}\int_x^{1/2}\frac{dy}{y}xP_{q\overline{q}\to\overline{q}}(x,y)yf^A_{q_i}(y,Q^2)yf^A_{\overline{q}_i}(y,Q^2)\\
&+A_{eff}\frac{\alpha_s^2(Q^2)}{4\pi R^2Q^2}\int_{x/2}^{x}\frac{dy}{y}xP_{q\overline{q}\to\overline{q}}(x,y)yf^A_{q_i}(y,Q^2)yf^A_{\overline{q}_i}(y,Q^2)\\
&-A_{eff}\frac{\alpha_s^2(Q^2)}{4\pi R^2Q^2}\int_x^{1/2}\frac{dy}{y}xP_{\overline{q}\overline{q}\to\overline{q}}(x,y)y[\Sigma^A(y,Q^2)-f^A_{q_i}(y,Q^2)]yf^A_{\overline{q}_i}(y,Q^2)\\
&+A_{eff}\frac{\alpha_s^2(Q^2)}{4\pi R^2Q^2}\int_{x/2}^{x}\frac{dy}{y}xP_{\overline{q}\overline{q}\to\overline{q}}(x,y)y[\Sigma^A(y,Q^2)-f^A_{q_i}(y,Q^2)]yf^A_{\overline{q}_i}(y,Q^2)\\
&-A_{eff}\frac{\alpha_s^2(Q^2)}{4\pi R^2Q^2}\int_x^{1/2}\frac{dy}{y}xP_{\overline{q}g\to\overline{q}}(x,y)yf^A_g(y,Q^2)yf^A_{\overline{q}_i}(y,Q^2)\\
&+A_{eff}\frac{\alpha_s^2(Q^2)}{4\pi R^2Q^2}\int_{x/2}^{x}\frac{dy}{y}xP_{\overline{q}g\to\overline{q}}(x,y)yf^A_g(y,Q^2)yf^A_{\overline{q}_i}(y,Q^2),(if\ x\le 1/2),
\end{aligned}
$$

$$
\begin{aligned}
&Q^2\frac{dxf^A_{\overline{q}_i}(x,Q^2)}{dQ^2}\\
&=\frac{\alpha_s(Q^2)}{2\pi}\int_x^1\frac{dy}{y}P_{qq}(z)xf^A_{\overline{q}_i}(y,Q^2)\\
&-\frac{\alpha_s(Q^2)}{2\pi}xf^A_{\overline{q}_i}(x,Q^2)\int_0^1 dzP_{qq}(z)\\
&+\frac{\alpha_s(Q^2)}{2\pi}\int_x^1\frac{dy}{y}P_{qg}(z)xf^A_g(y,Q^2)
\end{aligned}
$$

$$+A_{eff}\frac{\alpha_s^2(Q^2)}{4\pi R^2Q^2}\int_{x/2}^{1/2}\frac{dy}{y}xP_{gg\to\overline{q}}(x,y)[yf_g^A(y,Q^2)]^2$$

$$+A_{eff}\frac{\alpha_s^2(Q^2)}{4\pi R^2Q^2}\int_{x/2}^{1/2}\frac{dy}{y}xP_{q\overline{q}\to\overline{q}}(x,y)yf_{q_i}^A(y,Q^2)yf_{\overline{q}_i}^A(y,Q^2)$$

$$+A_{eff}\frac{\alpha_s^2(Q^2)}{4\pi R^2Q^2}\int_{x/2}^{1/2}\frac{dy}{y}xP_{\overline{q}q\to\overline{q}}(x,y)y[\Sigma^A(y,Q^2)-f_{q_i}^A(y,Q^2)]yf_{\overline{q}_i}^A(y,Q^2)$$

$$+A_{eff}\frac{\alpha_s^2(Q^2)}{4\pi R^2Q^2}\int_{x/2}^{1/2}\frac{dy}{y}xP_{\overline{q}g\to\overline{q}}(x,y)yf_g^A(y,Q^2)yf_{\overline{q}_i}^A(y,Q^2),(if\ 1/2\le x\le 1),\qquad(1-b)$$

for sea quark distributions and

$$Q^2\frac{dxf_g^A(x,Q^2)}{dQ^2}$$

$$=\frac{\alpha_s(Q^2)}{2\pi}\int_x^1\frac{dy}{y}P_{gq}(z)x\Sigma^A(y,Q^2)$$

$$+\frac{\alpha_s(Q^2)}{2\pi}\int_x^1\frac{dy}{y}P_{gg}(z)xf_g^A(y,Q^2)$$

$$-f\frac{\alpha_s(Q^2)}{2\pi}xf_g^A(x,Q^2)\int_0^1dzP_{qg}(z)$$

$$-\frac{1}{2}\frac{\alpha_s(Q^2)}{2\pi}xf_g^A(x,Q^2)\int_0^1dzP_{gg}(z)$$

$$-A_{eff}\frac{\alpha_s^2(Q^2)}{4\pi R^2Q^2}\int_x^{1/2}\frac{dy}{y}xP_{gg\to g}(x,y)[yf_g^A(y,Q^2)]^2$$

$$+A_{eff}\frac{\alpha_s^2(Q^2)}{4\pi R^2Q^2}\int_{x/2}^{x}\frac{dy}{y}xP_{gg\to g}(x,y)[yf_g^A(y,Q^2)]^2$$

$$-A_{eff}\frac{\alpha_s^2(Q^2)}{4\pi R^2Q^2}\int_x^{1/2}\frac{dy}{y}xP_{q\overline{q}\to g}(x,y)\sum_{i=1}^{f}[yf_{\overline{q}_i}^A(y,Q^2)]^2$$

$$+A_{eff}\frac{\alpha_s^2(Q^2)}{4\pi R^2Q^2}\int_{x/2}^{x}\frac{dy}{y}xP_{q\overline{q}\to g}(x,y)\sum_{i=1}^{f}[yf_{\overline{q}_i}^A(y,Q^2)]^2$$

$$-A_{eff}\frac{\alpha_s^2(Q^2)}{4\pi R^2Q^2}\int_x^{1/2}\frac{dy}{y}xP_{qg\to g}(x,y)y\Sigma^A(y,Q^2)yf_g^A(y,Q^2)$$

$$+A_{eff}\frac{\alpha_s^2(Q^2)}{4\pi R^2Q^2}\int_{x/2}^{x}\frac{dy}{y}xP_{qg\to g}(x,y)y\Sigma^A(y,Q^2)yf_g^A(y,Q^2),(if\ x\le 1/2),$$

$$Q^2\frac{dxf_g^A(x,Q^2)}{dQ^2}$$

$$= \frac{\alpha_s(Q^2)}{2\pi}\int_x^1 \frac{dy}{y} P_{gq}(z) x\Sigma^A(y,Q^2)$$

$$+\frac{\alpha_s(Q^2)}{2\pi}\int_x^1 \frac{dy}{y} P_{gg}(z) x f_g^A(y,Q^2)$$

$$-f\frac{\alpha_s(Q^2)}{2\pi} x f_g^A(x,Q^2)\int_0^1 dz P_{qg}(z)$$

$$-\frac{1}{2}\frac{\alpha_s(Q^2)}{2\pi} x f_g^A(x,Q^2)\int_0^1 dz P_{gg}(z)$$

$$+A_{eff}\frac{\alpha_s^2(Q^2)}{4\pi R^2 Q^2}\int_{x/2}^{1/2}\frac{dy}{y} x P_{gg\to g}(x,y)[y f_g^A(y,Q^2)]^2$$

$$+A_{eff}\frac{\alpha_s^2(Q^2)}{4\pi R^2 Q^2}\int_{x/2}^{1/2}\frac{dy}{y} x P_{q\overline{q}\to g}(x,y)\sum_{i=1}^{f}[y f_{\overline{q}_i}^A(y,Q^2)]^2$$

$$+A_{eff}\frac{\alpha_s^2(Q^2)}{4\pi R^2 Q^2}\int_{x/2}^{1/2}\frac{dy}{y} x P_{qg\to g}(x,y) y\Sigma^A(y,Q^2) y f_g^A(y,Q^2), (if\ 1/2 \le x \le 1), \quad (1-c)$$

for gluon distribution. The contributions of the negative nonlinear (shadowing) terms vanish in $0.5 < x < 1$. The coefficient $A_{eff} = 1 + \beta(A^{1/3} - 1)$; $(A^{1/3} - 1)$ is the number of shadowed nucleons. The fitting parameter $\beta = 0.21$, instead of 1, is due to the anisotropic two-dimensions distribution of nucleons in a Lorentz boost nucleus and the empty space among bound nucleons. Note that Eq. (1) dynamically produces the nuclear shadowing in quark- and gluon-distributions.

3 Fermi motion corrections

Generally, the EMC effect at large x is identified to the effect of the Fermi motion inside nucleus. This effect was studied by Bodek and Ritchie [10] and Frankfult and Strikman [11]. The Fermi motion smears the input quark distributions in a bound nucleon

$$F_2^A(x,\mu^2) = \int_{y\geq x} dy f_A^N(y) F_2^N(x/y,\mu^2), \tag{2}$$

where

$$f_A^N(y) = \frac{3m_N}{4k_F^3}[k_F^2 - m_N^2(y-\eta_A)^2], \tag{3}$$

for $\eta_A - k_F/m_N < y < \eta_A + k_F/m_N$; otherwise $f_A^N(y) = 0$. Here $\eta_A = 1 - B_A/m_N$ according to Fermi gas model. The average effective mass of the bound nucleons is $m_N^* = m_N - B_A$. The Fermi momentum k_F^A and the binding energy B_A take the values from nuclear physics (Table 1).

Table 1. The values of binding energy B_A taking from [12], the Fermi momentum taking from [10] and the swelling coefficient δ_A in Eq. (9).

Nuclei	Binding Energy B_A(MeV)	k_F(fm^{-1})	δ_A
^{2}H	1.10	0.6	0.01
^{4}He	7.07	1.03	0.055
^{7}Li	5.61	0.90	0.030
^{9}Be	6.46	1.06	0.055
^{12}C	7.68	1.12	0.055
^{27}Al	8.33	1.2	0.064
^{40}Ca	8.55	1.27	0.072
^{56}Fe	8.79	1.28	0.080
^{64}Gu	8.74	1.27	0.083
^{84}Kr	8.72	1.29	0.090
^{108}Ag	8.54	1.31	0.096
^{118}Sn	8.52	1.32	0.099
^{131}Xe	8.42	1.32	0.101
^{197}Au	7.92	1.35	0.112
^{208}Pb	7.87	1.36	0.113

Different from the binding model [13–15], we take B_A as the binding energy per nucleon ($\sim$ a few MeV) according to nuclear physics (see Table 1) rather than the separation energy ($20 \sim 40$ MeV). It implies that the bound nucleon is nearly on shell, since the nucleon consists of three valence quarks at μ-scale and hence without any extra component (pion) to balance the lost momentum in the off-mass shell effect. For detailed discussion see Ref. [16–19].

4 Nucleon swelling

After determining the dynamics of the EMC effect at small and large x regions, we focus on the EMC effect at the intermediate x region. We will choose a model from various present explanations about EMC effect [2].

The EMC effect at $0.3 < x < 0.7$ was explained in the traditional nuclear physics such as the binding model and pion model. However, the former was argued that it can not explain the EMC effect [20] by itself and later was ruled out due to the limits set by Drell-Yan measurements [21]. Besides, the high-precision experimental data on light nuclei from Jefferson Lab [22] suggests that the slope of $R(A/B)$ in the $0.3 < x < 0.7$ region depends on the location of the struck quark within nucleus, i.e., it is a local density effect. Therefore, the EMC effect can be described in terms of modifications to the internal partonic structure of the nucleon in the nuclear environment. One of such corrections is the swelling of bound nucleon [23, 24]. The presence of such structures within the bound nucleon could substantially increase the confinement radius. A natural result is deformation of the input parton distributions in a swelling nucleon according to the Heisenberg uncertainty principle. Such swelling mechanism was first discussed in a constituent quark model by Zhu and Shen in Ref. [16–19].

The simple three quark input distributions in Ref. [6] allow us easily to determine the nuclear deformed inputs. Particularly, the valence quark distributions in a proton and a bound nucleon in nucleus (A) at μ^2 are written as

$$xf_{v_u}^{p(A)}(x,\mu^2) = A_u^{p(A)} x^{B_u^{p(A)}} (1-x)^{C_u^{p(A)}},$$

$$xf_{v_d}^{p(A)}(x,\mu^2) = A_d^{p(A)} x^{B_d^{p(A)}} (1-x)^{C_d^{p(A)}}, \tag{4}$$

where the distributions in the proton are fixed in Ref. [6] as

$$xf_{v_u}^{p}(x,\mu^2) = 24.30 x^{1.98}(1-x)^{2.06},$$

and

$$xf_{v_d}^{p}(x,\mu^2) = 9.10 x^{1.31}(1-x)^{3.80}. \tag{5}$$

We define the dispersion of the input distributions as

$$D_u^{p(A)} = \left[\frac{1}{2} < f_{v_u}^{p(A)}(\mu^2) >_3 - \left(\frac{1}{2} < f_{v_u}^{p(A)}(\mu^2) >_2\right)^2\right]^{1/2}$$

$$D_d^{p(A)} = \left[< f_{v_d}^{p(A)}(\mu^2) >_3 - < f_{v_d}^{p(A)}(\mu^2) >_2^2\right]^{1/2}, \tag{6}$$

where $<>_n$ is the n-th moment of the distributions. The dispersion D^A decreases with the increased confinement scale of the initial valence quarks: $R_A = R_p + \delta R_A$ ($\delta R_A > 0$), according to the uncertainty principle. For $\delta R_A << R_p$ we have the following relation

$$D^A_{u(d)}(\mu^2)/D^p_{u(d)}(\mu^2) = R_p/R_A \equiv \frac{1}{1+\delta_A}. \tag{7}$$

The swelling of a bound nucleon arises from the nuclear force and relates to the local environment-the number of nucleons around it, since the nuclear force is a short distance interaction. Thus the A-dependence of swelling should be determined by the local properties of nuclear matter, i.e., the local nuclear density $\rho_A(r)$ ($\int \rho_A(r) d^3r = A$). We adopt the following simple way to estimate the swelling coefficient for $A > 12$

$$\delta_A = [1 - P_s(A)]\delta_0 + P_s(A)\delta_0/4, \tag{8}$$

where δ_0 is the swelling coefficient for a nucleon in the nuclear center. The second term is for the fact that the swelling of a nucleon on the nuclear surface is less than that of one in the interior: $1/2-$factor considers the average density of nucleon on the surface is about half of that in the nuclear kernel and the other $1/2$-factor is due to the space surround a nucleon on the nuclear surface, a half is vacuum and half is nuclear mater. $P_s(A)$ is the probability of a struck nucleon locating on the nuclear surface, and it can be estimated in terms of the nuclear density

$$\rho_A(r) = \rho_0/[1 + \exp[(r - R_A)/b]], \tag{9}$$

with $\rho_0 = 0.17$ nucleon/fm^3, $b = 0.54$ fm, and $R_A = 1.12A^{1/3} - 0.86A^{-1/3}$. The surface thickness is given by $D = (4\ln 5)b$. Thus,

$$P_s(A) = 1 - \int_0^{R_A-(D/2)} dr\rho_A(r)/A. \tag{10}$$

According to this picture, scattering from a central or deeply bound constituent gives a larger EMC effect than the scattering from a surface or weakly bound constituent. That is, the swelling effect is a local nuclear dynamical one. The free parameter $\delta_0 = 0.217$ is determined by the EMC ratio of any nucleus, for example, F_2^{Ca}/F_2^D.

5 The EMC effect

The EMC effect is exhibited in the ratio of the DIS structure function per nucleon bounded in a nucleus relative to that of deuterium D. In this work the isospin asymmetry is neglected. Therefore, we use F_2^{2H} to replace F_2^D, and the related parameters for $2H$ are listed in Table 1, where the k_f^{2H} is regarded as a parameter rather than the Fermi momentum since the gas model is unavailable. The ratio $R = F_2^{2H}/F_2^p$ is shown in Fig. 1.

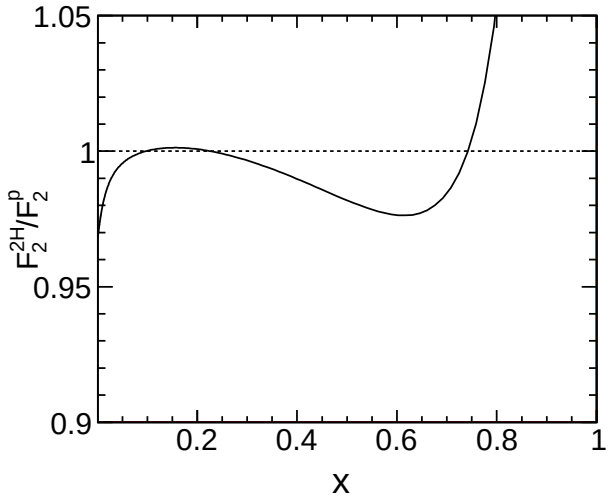

Figure 1: The isoscalar EMC effect ratio F_2^{2H}/F_2^p at $Q^2 = 5$ GeV^2.

There are four free parameters used in the determination of the proton parton distributions in our previous work [6]. In this work we add two free parameters: the coefficient $A_{eff} = 0.210$ and $\delta_0 = 0.217$ to predict the nuclear parton distributions. The other parameters in Table 1 are fixed by the knowledge of general nuclear physics.

With the above preparation, in Fig. 2 we present F_2^A/F_2^{2H} for various nuclei as a function of x at $Q^2 = 5$ GeV^2. The experimental data are taken from the publications by the European Muon Collaboration (EMC) [25, 26], the E49, E87, E139, and E140 Collaborations [27–30], the New Muon Collaboration (NMC) [31–34], BCDMS [35], HERMES [36] and Jefferson Lab [22].

As it can be seen, these ratios are in good agreement with the experimental data. The parton distributions of the proton are determined using the ZRS equation in [6]. It implies that we can not only predict the ratio of the structure functions, but also can give the absolute values of the nuclear structure functions themselves. These results are useful in the research of heavy ion collisions.

The nuclear dependence of the ratios in light nuclei ^4He, ^9Be and ^{12}C for $x > 0.2$ in Fig.3 presents that the EMC effect in this range depends on the local nuclear environment

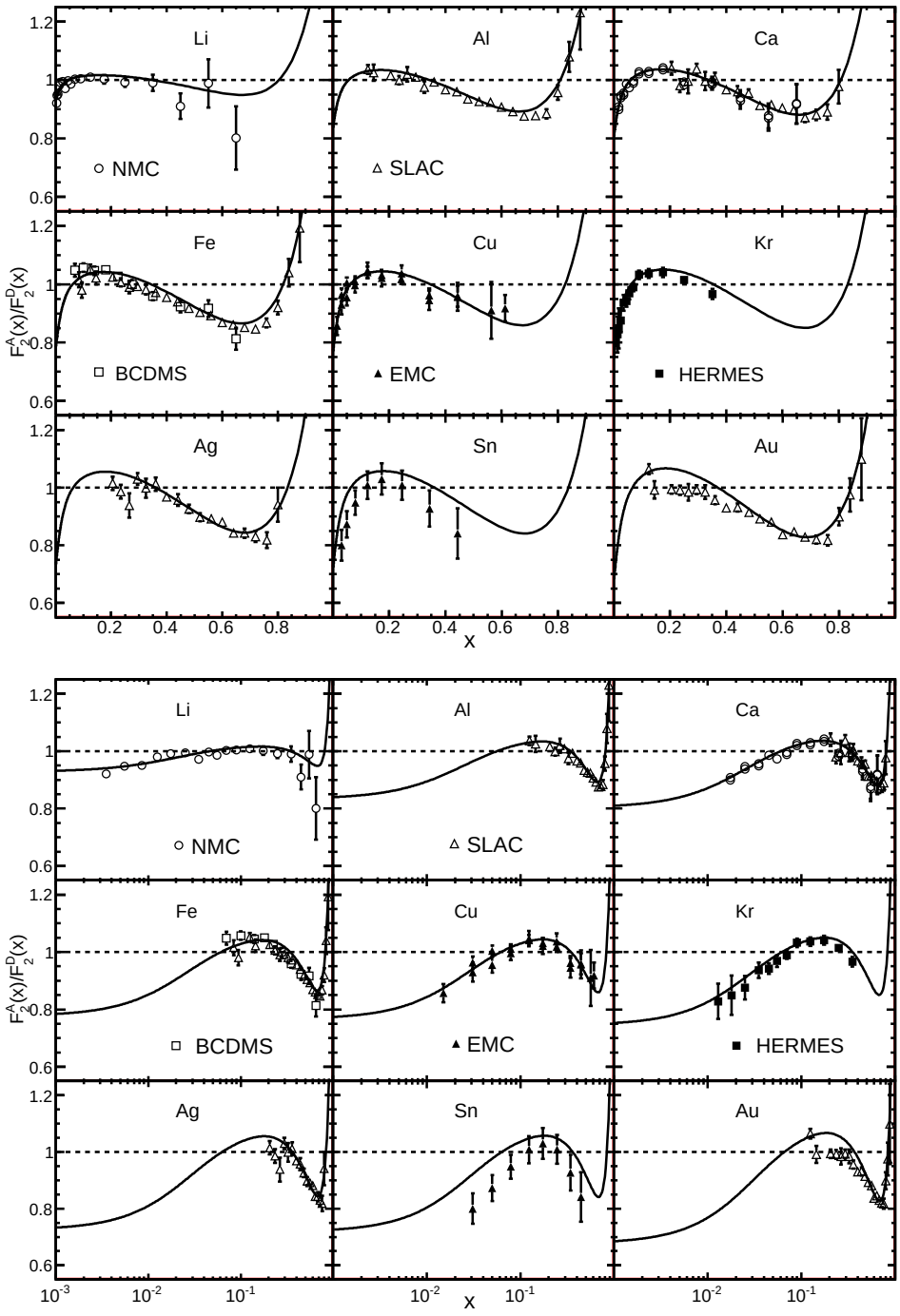

Figure 2: Predicted EMC effect ratios F_2^A/F_2^{2H} (solid curves) for various nuclei at $Q^2 = 5$ GeV^2 and comparisons with experimental data for F_2^A/F_2^D at $Q^2 > 1$ GeV^2. The upper and lower figures take different x scales but for the same results.

rather than on the average density. ^4He has similar average density with ^{12}C. While ^9Be is a special nucleus, which is constructed by a pair of tightly bound alpha particles plus one additional neutron [37] and most of its nucleons are in a dense environment, similar to ^4He. In consequence, we set $\delta_{He} \simeq \delta_{Be} \simeq \delta_C$. The clustering of nucleons in ^9Be leads to a special case where the average density does not reflect the local environment of the bulk of the nucleons.

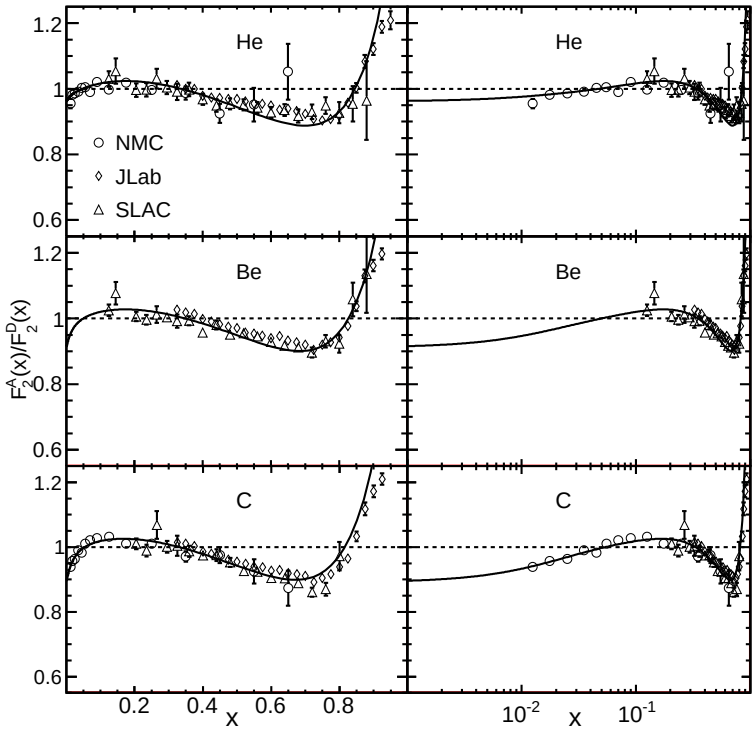

Figure 3: The structure function ratios for light nuclei. The solid curve is our theoretical predictions; (Left) and (Right) take different x scales but for the same results.

The NMC data [31–34] was measured simultaneously two different nuclear targets in one experiment with systematic errors being reduced significantly. Our predictions and comparisons with the NMC data are shown in Fig. 4. It is interesting that the ratios in Fig. 4 are finite at $x = 1$ if $k_F^A \sim k_F^B$ and it means that the ratios can be extended to $x > 1$. We call it the weak short range correlation (wSRC) [38–40] due to the Fermi motion.

Now let us discuss the structure of the EMC effect. We remove the contributions from bound nucleon swelling and Fermi motion effects in the ratio $R = F_2^{Ca}/F_2^D$. The remaining part in Figs. 5(a) and 5(b) is the shadowing and anti-shadowing effect. We find that the anti-shadowing effect contributes only a small fraction for the ratio in $0.05 < x < 0.3$ because it distributes in a broad x range. Note that the momentum conservation holds in Eq. (1) and the anti-shadowing effect is its dynamical result.

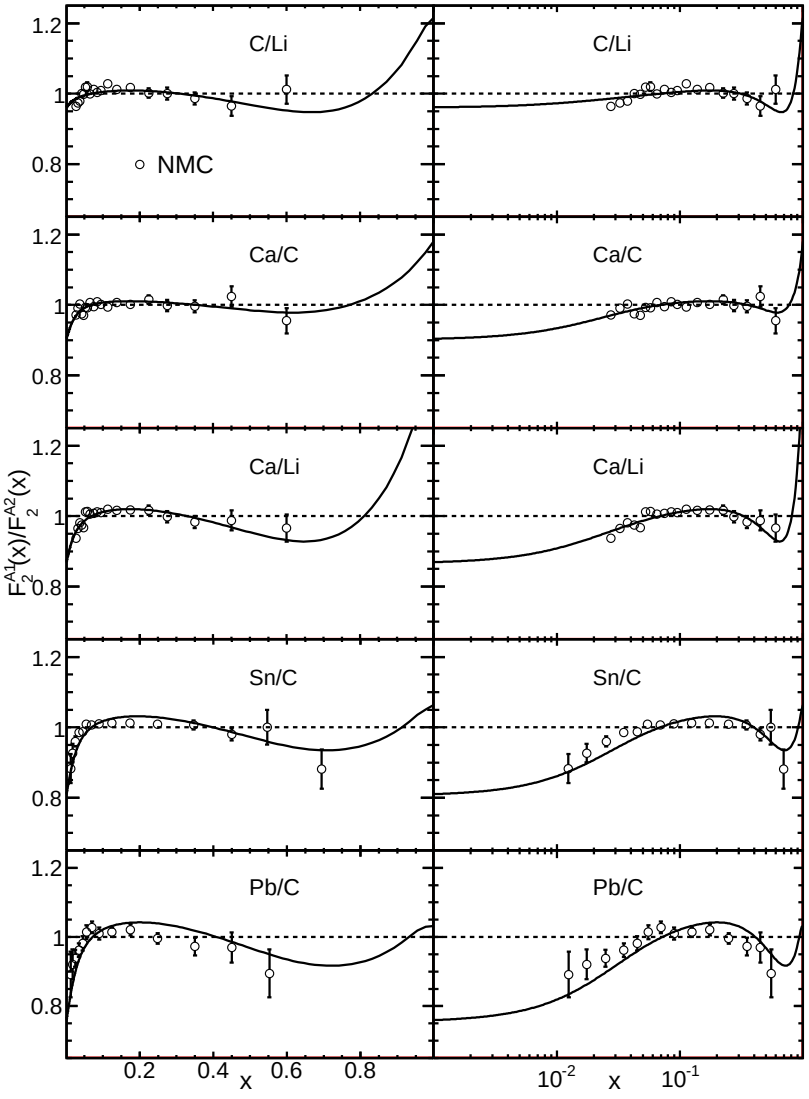

Figure 4: Our predicted structure function ratios $F_2^A/F_2^{A'}$ at $Q^2 = 5$ GeV^2 (solid curves) are compared with experimental data at $Q^2 > 2$ GeV^2.

For the Figs. 5(a) and 5(b), when we include the swelling effect, we get Figs. 5(c) and 5(d). The swelling effect enhances the distributions in the region $0.1 < x < 0.3$ and results in part of "anti-shadowing". This enhancement depends on the nuclear density (through δ_A) and, furthermore, does not disappear at large Q^2.

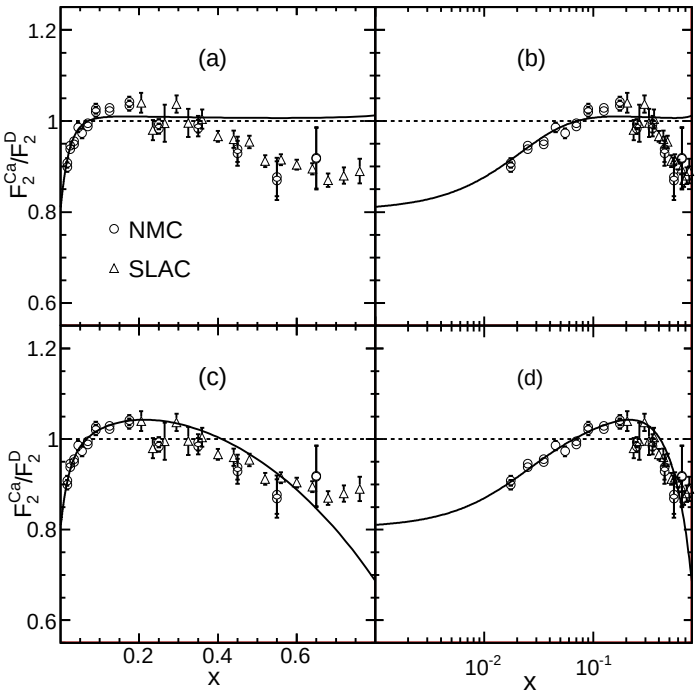

Figure 5: Nuclear shadowing and antishadowing contributions to the ratio F_2^{Ca}/F_2^D at $Q^2 = 5$ GeV^2 are shown in (a) and (b); The swelling effect is added in (c) and (d).

An example of theoretical prediction for the ratio $xf_g^{Ca}(x,Q^2)/xf_g^p(x,Q^2)$ at $Q^2 = 5$ GeV^2 in the nuclear gluon distribution is shown in Fig.6, where (a) and (b) are pure shadowing and anti-shadowing effect, in (c) and (d) swelling effect is added and (e) and (f) is the resulting EMC effect for gluon including Fermi motion. We find that both nuclear shadowing and anti-shadowing effect in the gluon distribution are not stronger than those in the quark distributions. In particular, we find a complicated structure of the EMC effect in $0.05 < x < 0.3$, where the anti-shadowing and swelling effects have different x- and Q^2-dependence.

Comparisons of our prediction $xf_g^{Pb}(x,Q^2)/xf_g^p(x,Q^2)$ at $Q^2 = 1.69$ GeV^2 for the gluon distributions with several DGLAP-based global models [41–44] are plotted in Fig. 7. Note that in the global analysis, the gluon distributions are mainly extracted by using the scaling violation. However, the experimental data about the EMC effect are restricted in a narrow Q^2 range at a fixed x. It would be rather difficult to pin down the nuclear gluon distributions in any global analysis. Besides, DGLAP equation works from

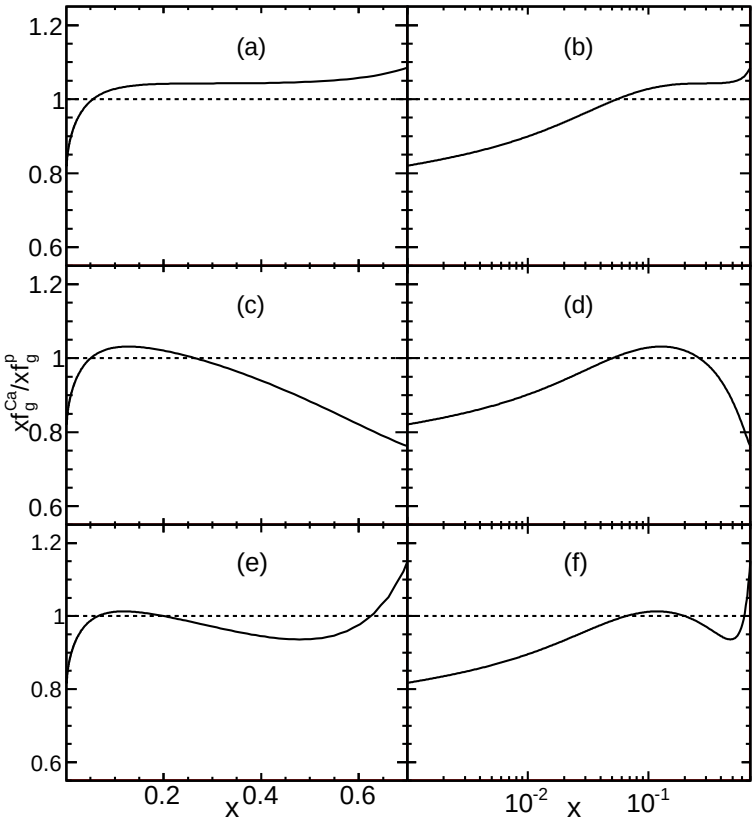

Figure 6: Nuclear shadowing and antishadowing contributions to the ratio xf_g^{Pb}/xf_g^p at $Q^2 = 5$ GeV^2 are shown in (a) and (b); The swelling effect is added in (c) and (d); A complete EMC effect (i.e., shadowing, antishadowing, swelling and Fermi motion) for gluon distribution ratio xf_g^{Ca}/xf_g^p is shown in (e) and (f).

a larger $Q^2 > 1$ GeV^2, where the x-dependent input distributions contain many *ad hoc* free parameters. Conversely, in this work the gluon distributions in either proton and nucleus are dynamically determined by Eq. (1), in which the input parameters are fixed by the proton structure functions and only a few extra free parameters are added for nucleus. One can expect that the uncertainty of nuclear gluon distributions in our work will be much reduced.

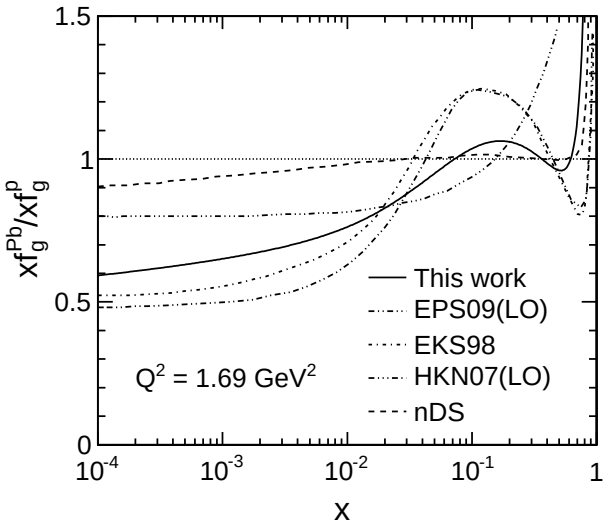

Figure 7: Comparisons of our prediction for xf_g^{Pb}/xf_g^p at $Q^2 = 1.69$ GeV^2 with the global models: EPS09 [41], EKS98 [42] (based on the leading-order (LO) global DGLAP analysis), HKN07 [43] and nDS [44] (next-to-leading-order (NLO) DGLAP analysis).

Finally, we present the ratio F_2^{Ca}/F_2^{2H} with various values of Q^2 in Fig.8. One can find that the Q^2-dependence of the EMC effect is weak at $x > 0.1$. It implies that it is reasonable to neglect Q^2-dependence in our work.

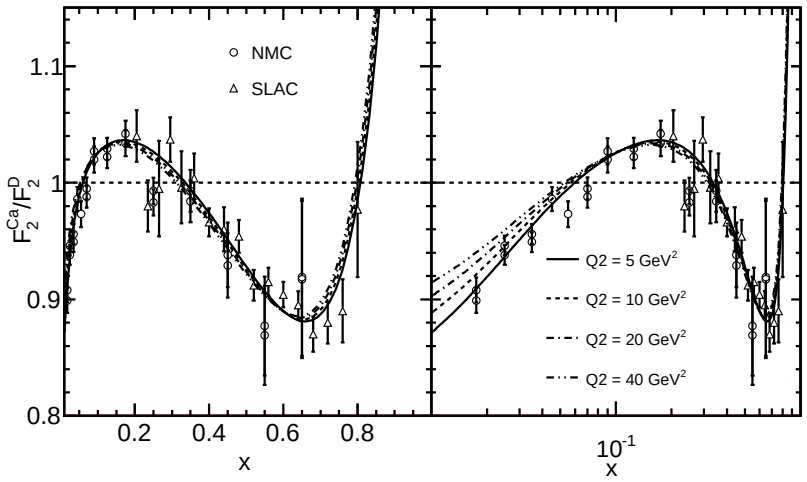

Figure 8: Q^2-dependence of the EMC effect for F_2^{Ca}/F_2^D, (Left) and (Right) take different x scales but for the same results.

6 Discussions and Conclusions

The main advantage of our explanation of the EMC effect comparing with the other models is that the parton distributions in both proton and nucleus are evolved according to a unified dynamics - the DGLAP equation with the ZRS corrections. The nuclear environment increases nonlinear effects and deforms the nonperturbative input quark distributions. In particular, the nuclear shadowing is a natural result of the QCD evolution rather than the parameterized description as in most of the EMC effect models. In consequence, the number of free parameters are much reduced in whole kinematic range. It implies that the prediction power of our approach for the nuclear parton distributions is enhanced.

In summary, we obtain new explanation on the EMC effect via the DGLAP equation with the ZRS corrections and minimum number of free parameters, where the nuclear shadowing effect is a dynamical evolution result of the equation, while nucleon swelling and Fermi motion in the nuclear environment deform the input parton distributions. In consequence, parton distributions of both proton and nucleus are predicted in a unified framework. We find that the parton recombination as a higher twist correction plays an essential role in the evolution of parton distributions either of proton or nucleus. We show a weak short range correlation if the Fermi momenta of two nuclei are closed. In particularly, the nuclear gluon distributions are dynamically predicted, which are important information for the recherche of the high energy nuclear physics.

Acknowledgments: This work is partly supported by the National Natural Science Foundations of China under the Grants Number 10875044, 11275120 and Century Pro-

gram of Chinese Academy of Sciences Y101020BR0.

References

[1] EMC Collab. (J. J. Aubert *et al.*), *Phys. Lett. B* **123** (1983) 275.

[2] M. Arneodo, *Phys. Rept.* **240** (1994) 301.

[3] F. E. Close, J. W. Qiu and R.G. Roberts, *Phys. Rev. D* **40** (1989) 2820.

[4] A.H. Mueller and J.W. Qiu, *Nucl. Phys. B* **268** (1986) 427.

[5] J.W. Qiu, *Nucl. Phys. B* **291** (1987) 746.

[6] X.R. Chen, J.H. Ruan, R. Wang, P.M. Zhang and W. Zhu, *Int. J. Mod. Phys. E* **23** (2014) 1450057 [arXiv:hep-ph/9809391].

[7] W. Zhu, *Nucl. Phys. B* **551**(1999) 245 [arXiv:hep-ph/9809391].

[8] W. Zhu, J.H. Ruan, *Nucl. Phys.B* **559** (1999) 378 [arXiv:hep-ph/9907330v2].

[9] W. Zhu and Z.Q. Shen, *HEP & NP,* **29** (2005) 109 [arXiv:hep-ph/0406213v3].

[10] A. Bodek and J. L. Ritchie, *Phys. Rev. D* **23** (1981) 1070.

[11] L.L. Frankfurt and M.I. Strikman, *Nucl. Phys. B* **181** (1981)22.

[12] M. Wang, G. Audi, A.H. Wapstra, F.G. Kondev, M. MacCormick, X. Xu and B. Pfeiffer, *CPC(HEP & NP).* **36**(2012)1603.

[13] C.H. Llewellyn Smith, *Phys. Lett. B* **128** (1983) 107.

[14] M. Ericson and A.W. Thomas, *Phys. Lett.B* **128**(1983) 112.

[15] E.L. Berger, F. Coester and R.B. Wiringa, *Phys. Rev. D* **29**(1984) 398.

[16] W. Zhu and J.G. Shen, *Phys. Lett. B* **219** (1989) 107.

[17] W. Zhu and J.G. Shen, *Phys. Lett. B* **235** (1990) 170.

[18] W. Zhu and J.G. Shen, *Phys. Rev. C* **41** (1990) 1674.

[19] W. Zhu and J.G. Shen, *Phys. Rev. C*, **43** (1991) 1996.

[20] J. R. Smith and G. A. Miller, *Phys. Rev.C* **65** (2002) 055206 [arXiv:nucl-th/0202016].

[21] D. M. Alde et al., *Phys. Rev. Lett.* **64** (1990) 2479.

[22] J. Seely, et al., *Phys. Rev. Lett.* **103** (2009) 202301 [arXiv:0904.4448].

[23] R.L. Jaffe, *Phys. Rev. Lett.* **50** (1983) 228.

[24] F.E. Close, R.G. Roberts and G.G. Ross, *Phys. Lett. B* **129** (1983) 346.

[25] EMC Collab. (J. Ashman *et al.*), *Phys. Lett. B* **202** (1988) 603.

[26] EMC Collab. (J. Ashman *et al.*), *Zeit. Phys. C* **57** (1993)211.

[27] E87 Collab. (A. Bodek *et al.*), *Phys. Rev. Lett.* **50**(1983) 1431.

[28] E49 Collab. (A. Bodek *et al.*), *Phys. Rev. Lett.* **51** (1983) 534.

[29] E140 Collab. (S. Dasu *et al.*), *Phys. Rev. Lett.* **60** (1988) 2591.

[30] E139 Collab. (J.Gomez *et al.*), *Phys. Rev.D* **49** (1994) 4348.

[31] NMC Collab. (P. Amaudruz *et al.*), *Nucl. Phys. B* **441** (1995) 3 [arXiv:hep-ph/9503291].

[32] NMC Collab. (P. Amaudruz *et al.*), *Z. Phys. C* **51** (1991) 387.

[33] NMC Collab. (M. Arneodo *et al.*), *Nucl. Phys. B* **481** (1996) 3.

[34] NMC Collab. (M. Arneodo *et al.*), *Nucl. Phys. B* **441** (1995) 12 [arXiv:hep-ex/9504002].

[35] BCDMS Collab.(Benvenuti *et al.*), *Phys. Lett. B* **189** (1987) 483.

[36] HERMES Collab. (K. Ackerstaff *et al.*), *Phys. Lett.B* **475** (2000) 386 [arXiv:hep-ex/9910071].

[37] K. Arai, Y. Ogawa, Y. Suzuki, and K. Varga, *Phys. Rev.C* **54** (1996) 132 [arXiv:nucl-th/9604009].

[38] L. L. Frankfurt and M. I. Strikman, *Phys. Rept.* **160** (1988) 235.

[39] L. Frankfurt and M. Strikman, *Int. J. Mod. Phys. E* **21** (2012) 1230002 [arXiv:hep-ph/1203.5278].

[40] O. Hen et al. *Int. J. Mod. Phys. E* **22** (2013) 1330017 [arXiv:nucl-th/1304.2813].

[41] K.J. Eskola, H. Paukkunen and C.A. Salgado, (EPS09), *JHEP* **4** (2009) 65 [arXiv:0902.4154].

[42] K.J. Eskola, V.J. Kolhinen and C.A. Salgado, *Eur, Phys. J.C.* **9** (1999) 61 [arXiv:hep-ph/9807297].

[43] M. Hirai, S. Kumano and T.H. Nagai, *Phys. Rev. C* **76** (2007) 065207 [arXiv:0709.3038].

[44] D. de Florian and R. Sassot, *Phys. Rev.D* **69** (2004) 074028 [arXiv:hep-ph/03112].